

**Observations of convective and dynamical instabilities in
tropopause folds and their contribution to
stratosphere-troposphere exchange**

John Y. N. Cho,¹ Reginald E. Newell,¹ T. Paul Bui,² Edward V. Browell,³ Marta A. Fenn,³ Bruce L. Gary,⁴ Michael J. Mahoney,⁴ Gerald L. Gregory,³ Glen W. Sachse,³ Stephanie A. Vay,³ Tom L. Kucsera,⁵ and Anne M. Thompson⁵

Version 11-30-98

Short title:

Abstract. With aircraft-mounted in-situ and remote sensing instruments for dynamical, thermal, and chemical measurements, we studied two cases of tropopause folding. In both folds we found Kelvin-Helmholtz billows with horizontal wavelength of about 900 m and thickness of about 120 m. In one case the instability was effectively mixing the bottomside of the fold, leading to the transfer of stratospheric air into the troposphere. Also we discovered in both cases small-scale secondary ozone maxima shortly after the aircraft ascended past the topside of the fold that corresponded to regions of convective instability. We interpreted this phenomenon as convectively breaking gravity waves. Therefore, we posit that convectively breaking gravity waves acting on tropopause folds must be added to the list of important irreversible mixing mechanisms leading to stratosphere-troposphere exchange.

Kelvin-Helmholtz waves

1. Introduction

At midlatitudes, tropopause folds are believed to be the major source of stratosphere-to-troposphere transfer of air. These V-shaped layers with high ozone and potential vorticity content angle down from the stratosphere for several kilometers and, at times, reach the planetary boundary layer. However, the fold itself is a reversible process, so for permanent stratosphere-troposphere exchange to take place the air in the fold must mix irreversibly with the outside environment. This necessary mixing has been attributed to Kelvin-Helmholtz-induced turbulence [Shapiro, 1980], boundary-layer turbulence [Johnson and Viezee, 1981], the folding of isentropic surfaces due to inertio-gravity waves [Danielsen *et al.*, 1991], wet convective erosion of the tropopause [World Meteorological Organization, 1986], and stratospheric streamer fragmentation [Appenzeller *et al.*, 1996]. However, few direct observations of the exchange process exist, and it is far from clear which, if any, of these proposed mixing mechanisms is dominant.

In this paper we present observations made through two tropopause folds with in-situ and remote sensing instruments aboard a DC-8 during the NASA subsonics assessment ozone and nitrogen experiment (SONEX) [Singh *et al.*, 1999]. Although the primary purpose of this mission was not the study of stratosphere-troposphere exchange, the extensive collection of chemical, dynamical, and thermal measurements in the upper troposphere enabled us to examine examples of tracer transport around tropopause folds.

2. Instrument Descriptions

SONEX was conducted between 1997-10-7 and 1997-11-10, and was aimed at studying the chemical effects of aircraft emissions in the North Atlantic flight corridor. The measurement platform was a DC-8 equipped with 16 scientific instruments.

Below we briefly describe the instruments relevant for this paper: the meteorological measurement system (MMS), the differential absorption lidar (DIAL), the microwave temperature profiler (MTP), the in-situ ozone probe, the differential absorption CO measurement (DACOM), and the laser hygrometer.

The MMS measured the air velocity with respect to the aircraft and the aircraft velocity with respect to the Earth, and combined the two vectors to get the zonal (u), meridional (v), and vertical (w) wind components. The air-motion system consisted of two 5-hole differential-pressure probes (Rosemount 858Y), three total-temperature probes with different response times, a pitot static-pressure probe, and a dedicated static-pressure system. The aircraft-motion sensing system consisted of a high-resolution inertial-navigation device (Litton LTN-72RH), an embedded GPS ring-laser inertial-navigation instrument (Litton LN-100G), and a multiple-antenna GPS attitude-reference system (Trimble TANS Vector). The data stream was sampled at 65 Hz, then subsequently reduced to 5 and 1 Hz for post-mission analysis. Pressure (p) and temperature (T) were also obtained from these probes, then potential temperature (θ) calculated from those values. The turbulent energy dissipation rate, ϵ , was estimated from the high-frequency wind data. For data accuracy, resolution, and the method for estimating ϵ , see *Chan et al.* [1998].

The DIAL system was used to remotely measure ozone and aerosols in the zenith and nadir directions. Two frequency-doubled Nd:YAG lasers were used to pump two frequency-doubled, tunable dye lasers. One of the dye lasers was operated at 292 nm for the DIAL on-line wavelength of ozone, and the other one was operated at 300 nm for the off-line wavelength. The output beams were transmitted out of the aircraft coaxially with the receiver telescopes. The backscattered laser energy was collected by two back-to-back 36-cm-diameter telescopes. The analog signals from the detectors were digitized at 5 MHz to a 12-bit accuracy, and the averaged digitized signals were stored every 2 s. The data sampling resolutions used in our study are 90 m in altitude and

60 s in time. More details on the system are available in previous publications [Browell, 1989; Browell et al., 1996].

The MTP, a passive microwave radiometer, measured the natural thermal emission from oxygen molecules at three frequencies (55.51, 56.66, and 58.79 GHz). It viewed ~~twenty~~ elevation angles between -80° and 80° using a scanning mirror, yielding a vertical temperature profile from near the surface to 24 km for each 16-s cycle. The altitude resolution was thus variable, with the best resolution of about ~~150~~⁵⁰ m near the aircraft level. The post-flight results were calibrated against available rawinsonde data. See Denning et al. [1989] for further information.

Ozone was measured in situ with the $\text{NO} + \text{O}_3$ chemiluminescence principle [Clough and Thrush, 1967]. Based on the sample exchange rate at sea level, the response time of the probe was estimated to be ~ 1 s with faster response at higher altitudes. Samples were taken at 6 Hz then averaged to 1 Hz. The data were further corrected for water-vapor quenching effects using the hygrometer measurements. The accuracy is estimated to be 5% or 2 ppbv, and the precision is estimated to be 2% or 0.8 ppbv.

The DACOM measured CO , N_2O , and CH_4 in situ with a folded-path, tunable diode-laser spectrometer using a differential absorption technique [Sachse et al., 1987; Collins et al., 1996]. Again the response time was estimated to be ~ 1 s based on the sample exchange rate. There were quasi-periodic gaps in the data of order 30 s every ~ 10 minutes due to the real-time calibration procedure, which was necessary to account for slow drifts in instrument sensitivity.

The laser hygrometer consisted of a compact laser transceiver mounted to an aircraft window plus a sheet of retroreflecting “road sign” material affixed to an outboard engine enclosure to complete the optical loop. Using differential absorption techniques, H_2O was sensed along this external path to an estimated precision of 2% in mixing ratio with a response time of 50 ms. By using a laser power normalization feature, the sensor was not affected by flying through clouds, haze, or aerosol plumes.

3. Observations

After two test flights out of its home base at Moffett Field, California, the DC-8 flew cross-country to Bangor, Maine on 13 October 1997. A prominent stratospheric intrusion was present over the north-central plains, and the DC-8 traversed its south end (Plate 1). The section of the tropopause fold penetrated by the aircraft was downstream of a trough and on the west side of a jet. Satellite images showed a clear column of air along the eastern flank of the intrusion bordered further east by a line of storm clouds associated with the accompanying upper-tropospheric front. While in the vicinity of the fold, the aircraft flew at a low altitude of ~ 6.5 km. However, the fold had extended even further below, and the DC-8 intersected it over northwestern Missouri as the aircraft ascended to ~ 11 km. Details will be shown and discussed in the next subsection.

Plate 1

During the next flight on 15 October 1997, the DC-8 encountered another stratospheric intrusion over the mid-Atlantic as it flew from Bangor to Shannon, Ireland (Plate 2). This time the fold existed on both the upstream and downstream sides of the trough. The aircraft, flying at ~ 3 km, passed through the lower tip of the western branch of the fold, then again traversed the same fold as it ascended steeply to over 7 km. It then entered the main body of the intrusion and ascended in steps as it crossed through to the eastern side. Again, the vertical cross-sectional view will be shown and discussed later.

Plate 2

Some of the subsequent flights during SONEX also sampled stratospheric intrusions, but we will focus our analysis on these two events because only in these cases did the aircraft ascend (or descend) through a tropopause fold giving us vertical profiles of data necessary for estimating high-resolution gradient and flux quantities.

3.1. Case 1: 13 October 1997

Plate 3 is a “curtain plot” of ozone concentration measured by the DIAL as the

Plate 3

DC-8 flew under, then up through the tropopause fold. The DC-8 was flying at a fairly constant air speed of $\sim 220 \text{ m s}^{-1}$ (the ground speed was slightly higher), so roughly 1 h corresponds to $\sim 800 \text{ km}$. Due to the incomplete overlap of the transmitted beam and the receiver field of view at close range, there was no data from the DIAL in the height range delineated by the dashed lines. In this region, the data was linearly interpolated by also including the in-situ measurement of ozone at the aircraft level; hence, the vertical blurring of the image in this zone. The apparent widening of the fold where the aircraft cut across it was probably not real.

In-situ measurements of trace gases reveal the fine structure present within the fold (Figure 1). The detailed anticorrelation of O_3 versus CO , N_2O , and H_2O show the intermingling of stratospheric and tropospheric air. (The CH_4 trace, not shown here, was virtually identical to that of CO .) Within what appeared to be the main body of the fold from about 18.04 to 18.09 UT, the gradient in the ozone concentration was mainly in the vertical (upward) direction. We deduce this from the observation that ozone remained steady as the aircraft was at level flight in the first half, while it increased as the aircraft ascended. Just after 18.06 UT when the aircraft began to ascend, there was a rapid oscillation in the trace constituent concentrations. We will argue later that this was a manifestation of a Kelvin-Helmholtz instability.

Figure 1

As the aircraft continued to climb, there was a secondary maximum in the ozone measurement (and minima in the other shown constituents) just after 18.11 UT. A possible third local maximum in ozone begins around 18.14 UT. The sharp edge on the topside of the main fold and this secondary maxima are reminiscent of past in-situ observations [Danielsen *et al.*, 1970; Shapiro, 1974; Danielsen and Mohnen, 1977; Johnson and Viezee, 1981]. These tropopause fold substructures have been attributed to low-frequency, short-vertical-wavelength inertio-gravity waves [Danielsen *et al.*, 1991] or differential advection by Rossby waves [Newman and Schoeberl, 1995]. Unfortunately, the resolution and the near-field blind zone of the DIAL did not allow us

to observe the two-dimensional character of these substructures.

The dynamical measurements are displayed in Figure 2. The increase in horizontal wind speed, especially in the meridional, as the aircraft ascended through then away from the fold is consistent with the classical picture of the jet stationed above the topside of the tropopause fold, inducing the secondary circulation necessary for folding. Clearly the background wind shear was quite strong in this region beneath the jet. The rapid oscillation seen just after 18.06 UT in the tracers are also visible here, especially in θ and u . Turbulence, as indicated by $\log \epsilon$, peaked at the edge of the main fold's topside (18.09 UT), around the second ozone maximum (~ 18.12 UT), and at the beginning of the third ozone maximum (just before 18.14 UT). There appears to be some correlation between ϵ , relative upward motion, and a decrease in $d\theta/dz$, which is suggestive of convective instability.

Figure 2

3.1.1. Dynamical (Kelvin-Helmholtz) instability. Let us now look closer at the rapid oscillations observed in both chemical and meteorological quantities shortly after 18.06 UT. Figure 3 shows the periodic undulations in tracer and dynamical measurements suggestive of Kelvin-Helmholtz (KH) billows. Note that because the chemical measurements were conducted at the end of long intake pipes, at these short time scales there were likely discernible delays relative to the MMS measurements that were taken by externally mounted probes. The perturbations in v were much smaller than in u , which is consistent with the plane of the vertical shear (estimated from the data to be 59° , measured clockwise from the north) being in closer alignment in the zonal direction than in the meridional direction.

Figure 3

Assuming that the oscillations were, indeed, KH billows, we can estimate their horizontal wavelength and vertical thickness. Along the aircraft heading, the period was about 5.5 s, which translates to a length of 1.23 km at the aircraft speed of 224 m s^{-1} . Since the aircraft heading was 102° , this yields a true horizontal wavelength of $\lambda_h = 1230 \cos(102^\circ - 59^\circ) = 900 \text{ m}$. The vertical thickness is then given by the

relationship, $\Delta z = \lambda_h/7.5 = 120$ m [Miles and Howard, 1964]. These numbers are quite similar to those of rapid oscillations observed near the tropopause by a uniquely high-resolution radar experiment [Cho *et al.*, 1996].

However, the calculated gradient Richardson number for the height interval across the presumed KH layer is $Ri = 0.52$, which is larger than the classic instability criterion of 0.25. It could be that the aircraft was already within the instability layer as it began its ascent, since the oscillation in the data began almost even before the climb began. If this were true, then the extra wind shear necessary to bring Ri down to 0.25 may have existed just below the aircraft height at 18.06 UT. Also, the instability may have been in a decay phase where Ri could be larger than 0.25. And, finally, because the aircraft flew more horizontally than vertically, horizontal gradients could have mapped into the estimated vertical gradients and acted against them. *awk*

Because the apparent KH instability occurred in the middle of the tropopause fold, it would not have been effective in mixing the air inside the fold with the air outside. Mainly it would have smoothed the vertical gradients of quantities within the instability layer. In terms of stratosphere-troposphere exchange we are more interested in turbulence occurring at the edge of the fold and also around the secondary maxima observed in ozone just outside the main fold region.

3.1.2. Convective (Rayleigh-Taylor) instability. We now turn our attention to the topside of the tropopause fold and to the secondary maxima in ozone that followed shortly. The bottomside of the fold was not associated with any appreciable turbulence, so we will not discuss it here.

Figure 4 shows the changes in the squares of the Brunt-Väisälä frequency, N , and vertical shear in horizontal winds, dU/dz , as well as the resulting Ri . For ease of comparison, we display $\log \epsilon$, w , and ozone concentration below them. To calculate the vertical gradients, we fit a straight line in a least-squares sense to the quantity versus altitude for an interval ± 60 m from the data point. This 120 m represents the largest

Figure 4

vertical eddy scale of turbulence, which can vary according to the flow conditions. However, it is a reasonable local value in light of the nearby observation of a dynamically unstable layer of the same thickness.

For potentially unstable regions as indicated by $Ri < 0.25$, there was a clear correspondence between high thermal stability (N^2) and high vertical shear. This preference for dynamic instability to occur across layers of enhanced thermal stability is in keeping with both theory [Phillips, 1966] and past observations [e.g., Fritts and Rastogi, 1985]. There was also a convectively unstable period between about 18.116 and 18.124 UT when N^2 and Ri became negative. Note that the vertical shear was very low during this time, which is consistent with the convective instability of high-frequency gravity waves in both theory and laboratory observations [Orlanski, 1972]. The same region experienced strong turbulence and large perturbations in upward velocity, which also points to convective instability. Furthermore, the gravity-wave breakdown interpretation is supported by a wavelike perturbation in u , v , and θ with maxima in the wind components and minima in $d\theta/dz$ at around 18.09 and 18.12 UT. Even the enhancements in fine-scale u and v perturbations at the “crests” are suggestive of wave breakdown. Although N^2 did not go negative around 18.09 UT, it did reach a local minimum. If the gravity-wave breakdown explanation is correct, then the secondary ozone maximum around 18.12 UT was probably the result of either vertical wave advection of the tropopause fold or upward, irreversible turbulent mixing of ozone or both.

Further evidence for convective instability around 18.12 UT comes from the MTP data. Figure 5 shows the temperature perturbation, T' , profiles as the aircraft flew through the tropopause fold region. Note that the aircraft went through an area of $dT'/dz < 0$ around 18.12 UT, i.e., an area made convectively less stable by the perturbation. Overall, there is a horizontally coherent, wavelike structure with a peak-to-peak amplitude of ~ 3 K.

Figure 5

3.1.3. Tropopause fold turbulent ozone flux. We can now estimate the vertical tracer flux from the tropopause fold to the ambient troposphere induced by turbulence generated by convective and dynamical instabilities. We will use ozone as the example tracer.

For a stably stratified ($N^2 > 0$) environment, we apply the vertical eddy diffusivity

$$K_z = \alpha \frac{\epsilon}{N^2} \quad (1)$$

where α is a proportionality factor that varies with the flow conditions [e.g., *Itsweire et al.*, 1986]. We invoke the expression derived by *Weinstock* [1992]

$$\alpha = 0.6 \left(\frac{L_e}{L_b} \right)^{\frac{4}{3}} e^{-0.51 \left(\frac{L_e}{L_b} \right)^{\frac{4}{3}}} \quad (2)$$

where $L_e = -2(2)^{1/2} \rho' (\partial \rho / \partial z)^{-1}$ is the vertical energy-containing scale of turbulence with ρ' the rms air density fluctuation and ρ the background air density, $L_b = 2\pi \epsilon^{1/2} N^{-3/2}$ is the buoyancy scale, and $L_\nu = 31\nu^{3/4} \epsilon^{-1/4}$ is the viscous dissipation scale with kinematic viscosity $\nu = 1.458 \times 10^{-6} T^{3/2} / [(T + 110.4)\rho]$ (Sutherland's formula). ρ can be calculated from p and T through the ideal gas law, $p = \rho RT$, where R is the gas constant for air.

For unstable and neutral conditions ($N^2 \leq 0$), we use

$$K_z = \beta \left(\frac{g |\Delta\theta| K_m^2}{\theta \nu} \right)^{\frac{1}{3}} \Delta z \quad (3)$$

where β is an empirical constant, g is the gravitational acceleration, $\Delta\theta$ and Δz are the vertical temperature difference and thickness across the unstable region, and K_m is the molecular diffusivity [*Kraichnan*, 1962; *Orlanski and Ross*, 1973]. We choose $\beta = 0.08$ following the laboratory results of *Ingersoll* [1966]. Using the relation $K_m/\nu = 1.34$ [*Chapman and Cowling*, 1970], Sutherland's formula, and the ideal gas law, (3) becomes

$$K_z = 1.57 \times 10^{-3} \left[\frac{g |\Delta\theta|}{\theta (T + 110.4) p} \right]^{\frac{1}{3}} T^{\frac{5}{6}} \Delta z \quad (4)$$

where p is in hPa. The vertical flux of trace constituent mixing ratio χ is then given by

$$\Phi_\chi = -K_z \frac{d\chi}{dz} \quad (5)$$

Figure 6 shows the resulting K_z and Φ_{O_3} calculated for the same period as covered by Figure 4. The ozone mixing ratio and its vertical gradient are also plotted for reference. The background gradient quantities were calculated in the same way as for Figure 4. Between about 18.115 and 18.125 UT when N^2 was less than or equal to 0, we took $|\Delta\theta| = 1.5$ K and $\Delta z = 225$ m for (4). K_z is relatively constant in this region, because the T and p fluctuations in (4) was much smaller than the ϵ fluctuations in (1). The largest ozone flux is upward from the topside of the “main” body of the tropopause fold, which is interesting since one usually thinks of stratosphere-to-troposphere transfer in terms of downward flux. The values are in excellent agreement with those estimated by *Shapiro* [1980] ($\Phi_{\text{O}_3} = 1.3\text{--}1.4$ m s⁻¹ ppbv on the topside of folds), which is remarkable considering that we used a completely different estimation method. The average value of $K_z = 4.4$ m² s⁻¹ calculated by *Danielsen et al.* [1987] from a simple three-dimensional model of a tropopause fold is somewhat larger than our values, but not very different considering the variability of the fold structure. We did not calculate Φ_{O_3} for the bottomside of the fold, because the aircraft was flying level there and we could not estimate the vertical gradient quantities. However, as seen in Figure 1 and Figure 2, the turbulence was very much weaker on the bottomside, so we believe the vertical mixing there was negligible.

Figure 6

3.2. Case 2: 15 October 1997

Plate 4 shows in color-scale form the vertical profiles of ozone concentration measured by the DIAL as the aircraft encountered the western branch of the tropopause fold (see also Plate 2). The apparent discontinuity in the fold was caused by the DIAL’s near-field blind zone marked by dashed lines in the figure. Thus, the fold was not visible inside the blind zone except where the aircraft intersected it with the in-situ probe. Following this “connect-the-dots” mental picture of the fold, one can see that the aircraft crossed it horizontally from topside to bottomside around 14.9 UT, then

Plate 4

ascended through it from bottomside to topside around 15.1 UT. This scenario is supported by the plot of stability as characterized by N^2 calculated from the MTP temperature profiles (Plate 5). Although instrumental problems cut off the data at 15.16 UT, we can still see the layer of very stable stratospheric air extending down from the righthand edge of the plot, leftward across the flight line around 15.1 UT, then down again through the flight path around 14.9 UT.

Plate 5

Figure 7 again shows the anticorrelation of O_3 versus CO and CH_4 , clearly indicating the encounter with a lower portion (height ~ 3 km) of the tropopause fold at around 14.9 UT and a higher section (height ~ 4 km) at 15.1 UT. The aircraft began entering the main body of the stratospheric intrusion around 15.4 UT. We note the similarity of the upper part of the fold to Case 1 in that the sharply defined topside was followed by a couple of weaker perturbations. There was also a hint of a wavelike structure in the ozone trace on the the more diffuse bottomside. Fortunately the aircraft was ascending through this region, so we will be able to estimate the vertical gradient quantities needed for instability analyses as we did for Case 1.

Figure 7

The corresponding dynamical measurements are displayed in Figure 8. In the ascent region of interest (15.05–15.3 UT), there was a zone of strong vertical shear and rapid oscillations in w around 15.1 UT corresponding to the second fold encounter. Together with the wavy bottomside seen in ozone, this suggests the presence of KH billows. Immediately following the shear zone was a fast oscillation in u that grew quickly with height and appeared to break around 15.14 UT corresponding to a maximum in ϵ and to the secondary ozone maxima. This combination of dynamical and tracer observations was also seen in Case 1, which we interpreted to be convectively breaking gravity waves. In this case the small-scale wave was superimposed on a larger-scale wave that also grew in amplitude with height and appeared to break around 15.3–15.4 UT. Note the strong enhancement in ϵ in this region. One can also see that $d\theta/dz$ was close to 0 in the areas of suspected convective wave breaking. With one-dimensional measurements such as we

Figure 8

have, it is not possible to unambiguously determine the wave parameters. Instead we will focus again on the instabilities themselves and their effects on the ozone flux.

Figure 9 is a blow-up plot of the second encounter with the tropopause fold. The oscillation was most clear in w while smaller perturbations with the same period were also visible in θ , v , and, to a lesser extent, in ozone. The perturbations in u were not closely correlated to those in w , which is consistent with the plane of the vertical shear (estimated from the data to be 163° , measured clockwise from the north) being in closer alignment in the meridional direction than in the zonal direction.

Again, assuming that the oscillations were KH billows, we can estimate their horizontal wavelength and vertical thickness. Along the aircraft heading, the period was about 25 s, which translates to a length of 5.2 km at the aircraft speed of 208 m s^{-1} . Since the aircraft heading was 82° , this yields a true horizontal wavelength of $\lambda_h = 5200 \cos(163^\circ - 82^\circ) = 810 \text{ m}$. The vertical thickness was then $\Delta z = \lambda_h/7.5 = 110 \text{ m}$. These numbers are remarkably close to those from Case 1.

One can readily see the mixing effects of the KH instability on the fold in the ozone measurement (Figure 9). The bottomside of the ozone maximum was much more diffuse than the topside. The ozone flux will be estimated shortly.

As in Case 1 we can calculate N^2 , the vertical shear, and Ri . These are shown in Figure 10. Again, there was a correspondence between regions of high shear and high thermal stability, conditions typically associated with KH instability. Ri did fall close to or below 0.25 during the period of the suspected KH billows (15.085–15.115 UT), and as with Case 1 there was a region of negative N^2 ($\sim 15.14 \text{ UT}$) associated with a secondary ozone maximum and apparent wave-breaking (as discussed above).

Finally we estimate the vertical ozone flux for this period (Figure 11). Where $N^2 < 0$ around 15.15 UT, we took $|\Delta\theta| = 0.8 \text{ K}$ and $\Delta z = 80 \text{ m}$ for (4). The flux values are generally lower than for Case 1. This is not surprising since the turbulence was weaker and the ozone gradients were smaller. Since the altitude of fold interception

Figure 9

Figure 10

Figure 11

was lower in Case 2 (~ 4 km) than in Case 1 (~ 6.5 km), the stratospheric air inside the fold would have had more time to mix with the surrounding tropospheric air, thus weakening the ozone gradient at the edges. This can also be seen in the peak ozone concentration inside the folds, ~ 110 ppbv for Case 2 versus ~ 190 ppbv for Case 1.

4. Summary Discussion

Even though the two cases of tropopause folding studied here occurred at different times and places, and were sampled at different altitudes, there were some striking similarities. Both folds had sharply defined topsides with two fold-like substructures shortly following containing lower ozone amounts than the fold itself. It is difficult to say whether these substructures were horizontal or vertical variations because the flight paths were one-dimensional and slantwise. Unfortunately the near-field blind zone and coarse time resolution of the DIAL did not allow two-dimensional mapping of these small-scale ozone perturbations. If the perturbations were purely horizontal, then their separation distances would have been about 10 and 8 km for Case 1 and Case 2. If they were purely vertical, then their separation distances were about 400 and 200 m, respectively. Of course, the reality could have been somewhere in between the two extremes. Because in both cases the first of these substructures was associated with convective instability and turbulence, and because there were wavelike perturbations in the wind and temperature corresponding to the ozone substructures, we proposed convectively breaking gravity waves to explain the data. It then follows that the substructures were mostly horizontal perturbations, since convective breakdown occurs in high-frequency gravity waves (KH instability sets in first for low-frequency gravity waves) [*Fritts and Rastogi*, 1985] and high-frequency gravity waves cannot have such short vertical wavelengths. Thus, we conclude that the substructural phenomenon we observed was different from the thin ozone laminae interpreted by *Danielsen et al.* [1991] as inertio-gravity waves and by *Newman and Schoeberl* [1995] as Rossby-wave-induced

differential advection.

Although laboratory measurements and numerical studies confirm the existence of convective gravity-wave breakdown, direct atmospheric observations have largely been lacking due to the difficulty in making the required high-resolution measurements. However, convective instability is believed to play a crucial role in gravity-wave saturation [e.g., *Dunkerton*, 1989; *Andreassen et al.*, 1994]. Originally proposed by *Hodges* [1967], saturation theory calls for the natural growth of upward-propagating gravity waves to be limited by various instabilities and/or diffusive damping/filtering mechanisms [e.g., *Gardner*, 1996]. Thus, it is important to obtain more direct evidence that convective gravity-wave breakdown does occur in the atmosphere, and to pinpoint the conditions under which they proceed. In this study we showed observational examples of convective gravity-wave breaking, and, for those cases, they appeared to occur preferentially just above a tropopause fold. This could be because the θ surfaces are moved further apart vertically (thus weakening the static stability) on the cyclonic flank of a jet corresponding to where the tropopause fold is created. Also the rapid increase in horizontal velocity with height underneath the jet lowers the amplitude threshold for wave breaking [*Thorpe*, 1978] and causes more gravity waves with phase velocities in the same direction as the background flow to reach critical levels and convective instability [*Thorpe*, 1981; *Fritts*, 1982]. In any case, we need to add convectively breaking gravity waves to the list of mechanisms leading to the irreversible mixing of tropopause folds with their environment.

KH instabilities are much more commonly observed in the atmosphere (see, e.g., *Fritts and Rastogi* [1985] for references). We observed KH billows inside both tropopause folds encountered, and noted a correlation between strong vertical shear and high static stability as anticipated theoretically [*Phillips*, 1966] and observed frequently [e.g., *Browning et al.*, 1973]. In Case 2, the KH instability had apparently acted on the bottomside ozone gradient and made it much more diffuse than the topside of the fold,

whereas in Case 1 the KH instability located in the middle of the fold was not effective in mixing air inside and outside the fold.

The site of maximum ozone flux out of a tropopause fold was on the topside of Case 1, with a peak value of about $1.5 \text{ ppbv m s}^{-1}$ in good agreement with previous aircraft observations by *Shapiro* [1980]. In this particular case, the instability was generated by a combination of background shear and wave-induced weakening of static stability. However, we must insert a cautionary note regarding our estimates of K_z and Φ_{O_3} . The method of estimating ϵ from 5-Hz dynamical measurements as outlined by *Chan et al.* [1998] has not been fully verified by comparison with other instruments. However, we decided to use this approach because the 1-s resolution of the tracer measurements was not fine enough for a direct $\overline{w'\chi'}$ approach. In 1 s the aircraft traverses over 200 m, so the Nyquist length scale would be greater than the turbulent eddy scale. So $\overline{w'\chi'}$ would not represent turbulent flux, which is what we wanted in our investigation of irreversible transport. Also (3) is not the only eddy diffusion formulation proposed for convective turbulence. For example, $K_z \sim |N|$ has also been suggested [*Priestley*, 1954; *Lilly*, 1962], which yields much higher K_z values for our two cases. So there is considerable uncertainty in eddy diffusivity under convective turbulence. But there are theoretical reasons and experimental evidence favoring (3) [*Globe and Dropkin*, 1959; *Kraichnan*, 1962; *Ingersoll*, 1966].

Acknowledgments. The work at M.I.T. was funded by NASA grant NAG2-1105.

The work performed by MSM was carried out ~~out~~ by The Jet Propulsion Laboratory, California Institute of Technology, under a contract with the National Aeronautics and Space Administration.

References

- Andreassen, Ø., C. E. Wasberg, D. C. Fritts, and J. R. Isler, Gravity wave breaking in two and three dimensions. 1: Model description and comparison of two-dimensional evolutions, *J. Geophys. Res.*, *99*, 8095–8108, 1994.
- Appenzeller, C., H. C. Davies, and W. A. Norton, Fragmentation of stratospheric intrusions, *J. Geophys. Res.*, *101*, 1435–1456, 1996.
- Browell, E. V., Differential absorption lidar sensing of ozone, *Proc. IEEE*, *77*, 419–432, 1989.
- Browell, E. V., M. A. Fenn, C. F. Butler, W. B. Grant, M. B. Clayton, J. Fishman, A. S. Bachmeier, B. E. Anderson, G. L. Gregory, H. E. Fuelberg, J. D. Bradshaw, S. T. Sandholm, D. R. Blake, B. G. Heikes, G. W. Sachse, H. B. Singh, and R. W. Talbot, Ozone and aerosol distributions and air mass characteristics over the South Atlantic Basin during the burning season, *J. Geophys. Res.*, *101*, 24,043–24,068, 1996.
- Browning, K. A., G. W. Bryant, J. R. Starr, and D. N. Axford, Air motion within Kelvin-Helmholtz billows determined from simultaneous Doppler radar and aircraft measurements, *Q. J. R. Meteorol. Soc.*, *99*, 608–618, 1973.
- Chan, K. R., J. Dean-Day, S. W. Bowen, and T. P. Bui, Turbulence measurements by the DC-8 meteorological measurement system, *Geophys. Res. Lett.*, *25*, 1355–1358, 1998.
- Chapman, S., and T. G. Cowling, *The Mathematical Theory of Non-Uniform Gases*, 423 pp., Cambridge Univ. Press, New York, 1970.
- Cho, J. Y. N., R. F. Jurgens, and M. A. Slade, High-resolution stratospheric dynamics measurements with the NASA/JPL Goldstone solar system radar, *Geophys. Res. Lett.*, *23*, 1909–1912, 1996.
- Clough, P. N., and B. A. Thrush, Mechanism of chemiluminescent reaction between nitric oxide and ozone, *Trans. Faraday Soc.*, *63*, 915–925, 1967.
- Collins, J. E., G. W. Sachse, B. E. Anderson, R. C. Harriss, K. B. Bartlett, S. T. Sandholm, L. O. Wade, L. G. Burney, and G. F. Hill, Airborne nitrous oxide observations over

- the western Pacific Ocean: September-October 1991, *J. Geophys. Res.*, *101*, 1975-1984, 1996.
- Danielsen, E. F., R. Bleck, J. Shedlovsky, A. Wartburg, P. Haagenson, and W. Pollock, Observed distribution of radioactivity, ozone, and potential vorticity associated with tropopause folding, *J. Geophys. Res.*, *75*, 2353-2361, 1970.
- Danielsen, E. F., R. S. Hipskind, S. E. Gaines, G. W. Sachse, G. L. Gregory, and G. F. Hill, Three-dimensional analysis of potential vorticity associated with tropopause folds and observed variations of ozone and carbon monoxide, *J. Geophys. Res.*, *92*, 2103-2111, 1987.
- Danielsen, E. F., R. S. Hipskind, W. L. Starr, J. F. Vedder, S. E. Gaines, D. Kley, and K. K. Kelly, Irreversible transport in the stratosphere by internal waves of short vertical wavelength, *J. Geophys. Res.*, *96*, 17,433-17,452, 1991.
- Danielsen, E. F., and V. A. Mohnen, Project Duststorm report: Ozone transport, in situ measurements, and meteorological analyses of tropopause folding, *J. Geophys. Res.*, *82*, 5867-5877, 1977.
- Denning, R. F., S. L. Guidero, G. S. Parks, and B. L. Gary, Instrument description of the airborne microwave temperature profiler, *J. Geophys. Res.*, *94*, 16,757-16,766, 1989.
- Dunkerton, T. J., Theory of internal gravity wave saturation, *Pure Appl. Geophys.*, *130*, 373-397, 1989.
- Fritts, D. C., The transient critical-level interaction in a Boussinesq fluid, *J. Geophys. Res.*, *87*, 7997-8013, 1982.
- Fritts, D. C., and P. K. Rastogi, Convective and dynamical instabilities due to gravity wave motions in the lower and middle atmosphere: Theory and observations, *Radio Sci.*, *20*, 1247-1277, 1985.
- Gardner, C. S., Testing theories of atmospheric gravity wave saturation and dissipation, *J. Atmos. Terr. Phys.*, *58*, 1575-1589, 1996.

- Globe, S., and D. Dropkin, Natural convection heat transfer in liquids confined by two horizontal plates and heated from below, *J. Heat Transfer*, 81, 156–185, 1959.
- Hodges, R., Generation of turbulence in the upper atmosphere by internal gravity waves, *J. Geophys. Res.*, 72, 3455–3458, 1967.
- Ingersoll, A. P., Thermal convection with shear at high Rayleigh number, *J. Fluid Mech.*, 25, 209–228, 1966.
- Itsweire, E. C., K. N. Helland, and C. W. Van Atta, The evolution of grid-generated turbulence in stratified fluid, *J. Fluid Mech.*, 126, 299–338, 1986.
- Johnson, W. B., and W. Viezee, Stratospheric ozone in the lower troposphere—I. Presentation and interpretation of aircraft measurements, *Atmos. Environ.*, 15, 1309–1323, 1981.
- Kraichnan, R., Turbulent thermal convection at arbitrary Prandl number, *Phys. Fluids*, 5, 1374–1389, 1962.
- Lilly, D. K., On the numerical simulation of buoyant convection, *Tellus*, 14, 148–172, 1962.
- Miles, J. W., and L. N. Howard, Note on a heterogeneous shear flow, *J. Fluid Mech.*, 20, 331–336, 1964.
- Newman, P. A., and M. R. Schoeberl, A reinterpretation of the data from the NASA stratosphere-troposphere exchange project, *J. Geophys. Res.*, 22, 2501–2504, 1995.
- Orlanski, I., On the breaking of standing internal gravity waves, *J. Fluid Mech.*, 54, 577–598, 1972.
- Orlanski, I., and B. B. Ross, Numerical simulation of the generation and breaking of internal gravity waves, *J. Geophys. Res.*, 78, 8808–8826, 1973.
- Phillips, O. M., *The Dynamics of the Upper Ocean*, 261 pp., Cambridge Univ. Press, New York, 1966.
- Priestley, C. H. B., Convection from a horizontal surface, *Aust. J. Phys.*, 7, 176–201, 1954.

- Sachse, G. W., G. F. Hill, L. O. Wade, and M. G. Perry, Fast-response, high precision carbon monoxide sensor using a tunable diode laser absorption technique, *J. Geophys. Res.*, *92*, 2071–2081, 1987.
- Shapiro, M. A., A multiple-structured frontal zone-jet stream system as revealed by meteorologically instrumented aircraft, *Mon. Weath. Rev.*, *102*, 244–253, 1974.
- Shapiro, M. A., Turbulent mixing within tropopause folds as a mechanism for the exchange of chemical constituents between the stratosphere and troposphere, *J. Atmos. Sci.*, *37*, 994–1004, 1980.
- Singh, H. B., A. M. Thompson, and J. A. Eilers, An overview of SONEX 1997, *Geophys. Res. Lett.*, 1999, in preparation.
- Thorpe, S. A., On the shape and breaking of finite amplitude gravity waves in a shear flow, *J. Fluid Mech.*, *85*, 7–31, 1978.
- Thorpe, S. A., An experimental study of critical layers, *J. Fluid Mech.*, *103*, 321–344, 1981.
- Weinstock, J., Vertical diffusivity and overturning length in stably stratified turbulence, *J. Geophys. Res.*, *97*, 12,653–12,658, 1992.
- World Meteorological Organization, *Atmospheric Ozone 1985*, WMO Report No. 16. World Meteorological Organization, Case Postale No. 5, Geneva, 1986.

E. V. Browell, M. A. Fenn, G. L. Gregory, G. W. Sachse, and S. A. Vay,
NASA Langley Research Center, 21 Langley Blvd., Hampton, VA 23681-2199.
(e-mail: e.v.browell@larc.nasa.gov; m.a.fenn@larc.nasa.gov; g.l.gregory@larc.nasa.gov;
g.w.sachse@larc.nasa.gov; s.a.vay@larc.nasa.gov)

T. P. Bui, Mail Stop 245-5, NASA Ames Research Center, Moffett Field, CA
94035-1000. (e-mail: bui@mms.arc.nasa.gov)

J. Y. N. Cho (corresponding author) and R. E. Newell, Department of Earth,
Atmospheric, and Planetary Sciences, Massachusetts Institute of Technology,

77 Massachusetts Ave., Rm. 54-1823, Cambridge, MA 02139-4307. (e-mail: jcho@pemtropics.mit.edu; newell@newell1.mit.edu)

~~B. L. Gary~~ and M. J. Mahoney, Mail Stop ²⁴⁶⁻¹⁰¹~~168-214~~, NASA Jet Propulsion Laboratory, ^{California Institute of Technology,} 4800 Oak Grove Dr., Pasadena, CA 91109-8099. (e-mail: ~~bgary@jpl.nasa.gov;~~ michael.j.mahoney@jpl.nasa.gov)

T. L. Kucsera, A. M. Thompson, Code 916, NASA Goddard Space Flight Center, Greenbelt Rd., Greenbelt, MD 20771-0001. (e-mail: tlk@croc.gsfc.nasa.gov; thompson@gator1.gsfc.nasa.gov)

Received _____

¹Department of Earth, Atmospheric, and Planetary Sciences, Massachusetts Institute of Technology, Cambridge.

²NASA Ames Research Center, Moffett Field, California.

³NASA Langley Research Center, Hampton, Virginia.

⁴NASA Jet Propulsion Laboratory, Pasadena, California.

⁵NASA Goddard Space Flight Center, Greenbelt, Maryland.

Figure 1. Plots of O_3 (first panel), CO (second panel), N_2O (third panel), and H_2O (fourth panel) mixing ratios through the tropopause fold region on 13 October 1997. The bottom panel shows the pressure altitude of the aircraft.

Figure 2. Plots of u (first panel), v (second panel), w (third panel), $\log \epsilon$ (fourth panel), and θ (fifth panel) through the tropopause fold region on 13 October 1997.

Figure 3. Expanded time plots of O_3 (first panel), CO (second panel), N_2O (third panel), H_2O (fourth panel), u (fifth panel), v (sixth panel), w (seventh panel), θ (eighth panel), and $\log \epsilon$ (ninth panel) from 13 October 1997.

Figure 4. Plots of N^2 (first panel), $(dU/dz)^2$ (second panel), Ri (third panel), $\log \epsilon$ (fourth panel), w (fifth panel), and O_3 mixing ratio (sixth panel) from 13 October 1997.

Figure 5. Temperature perturbation profiles (solid lines) calculated from the MTP. A straight line was fitted to the measured temperature profile in a least-squares sense over the height range depicted by each line in the figure, then that trend was subtracted from the profile. The dashed line indicates the altitude of the aircraft.

Figure 6. Plots of O_3 mixing ratio (first panel), vertical gradient of O_3 mixing ratio (second panel), K_z (third panel), and vertical flux of O_3 mixing ratio (fourth panel) from 13 October 1997.

Figure 7. Plots of O_3 (first panel), CO (second panel), and CH_4 (third panel) mixing ratios through the two intersections with the western branch of the tropopause fold region on 15 October 1997. The bottom panel shows the pressure altitude of the aircraft.

Figure 8. Plots of u (first panel), v (second panel), w (third panel), $\log \epsilon$ (fourth panel), and θ (fifth panel) through the two intersections with the western branch of the tropopause fold region on 15 October 1997.

Figure 9. Expanded time plots of O_3 (first panel), u (second panel), v (third panel), w (fourth panel), and θ (fifth panel) from 15 October 1997.

Figure 10. Plots of N^2 (first panel), $(dU/dz)^2$ (second panel), Ri (third panel), $\log \epsilon$ (fourth panel), w (fifth panel), and O_3 mixing ratio (sixth panel) from 15 October 1997.

Figure 11. Plots of O_3 mixing ratio (first panel), vertical gradient of O_3 mixing ratio (second panel), K_z (third panel), and vertical flux of O_3 mixing ratio (fourth panel) from 15 October 1997.

Plate 1. Map of geopotential height (blue contour lines), modified potential vorticity (color scale), and horizontal winds (yellow vectors) on the 330-K surface for 1200 UT, 13 October 1997. The plotted field values were output from a model run by the Data Assimilation Office of the NASA Goddard Space Flight Center. The longitudinal and latitudinal grid spacing used by the model was 2.5° by 2° . The white line shows the flight path of the DC-8, which departed Moffett Field, California at 1519 UT and landed in Bangor, Maine at 2241 UT.

Plate 2. Same as Plate 1 except for 15 October 1997. The DC-8 departed Bangor at 1211 UT and landed in Shannon, Ireland at 1821 UT.

Plate 3. DIAL ozone measurements made in the vicinity of the tropopause fold over the central United States on 13 October 1997. The black solid line shows the altitude of the aircraft, and the dashed black lines demarcate the zone of no data. In this region the data was linearly interpolated including also the in-situ ozone measurement at aircraft level. There was also missing data between 17.7 UT and 17.8 UT. The position of the aircraft at the beginning of the plot was 39.6°N , 103.3°W and 39.0°N , 92.0°W at the end of the plot. Its heading did not change much between those two points.

Plate 4. DIAL ozone measurements made in the vicinity of the western branch of the tropopause fold over the north Atlantic on 15 October 1997. The white solid line shows the altitude of the aircraft, and the dashed white lines demarcate the zone of no data. In this region the data was linearly interpolated including also the in-situ ozone measurement at aircraft level. The position of the aircraft at the beginning of the plot was 55.0°N, 48.7°W and 55.4°N, 36.8°W at the end of the plot. Its heading did not change much between those two points.

Plate 5. Vertical profiles of N^2 calculated from the MTP temperature data on 15 October 1997. The aircraft flight level is indicated by the black solid line.

SONEX DC-8 1997/10/13

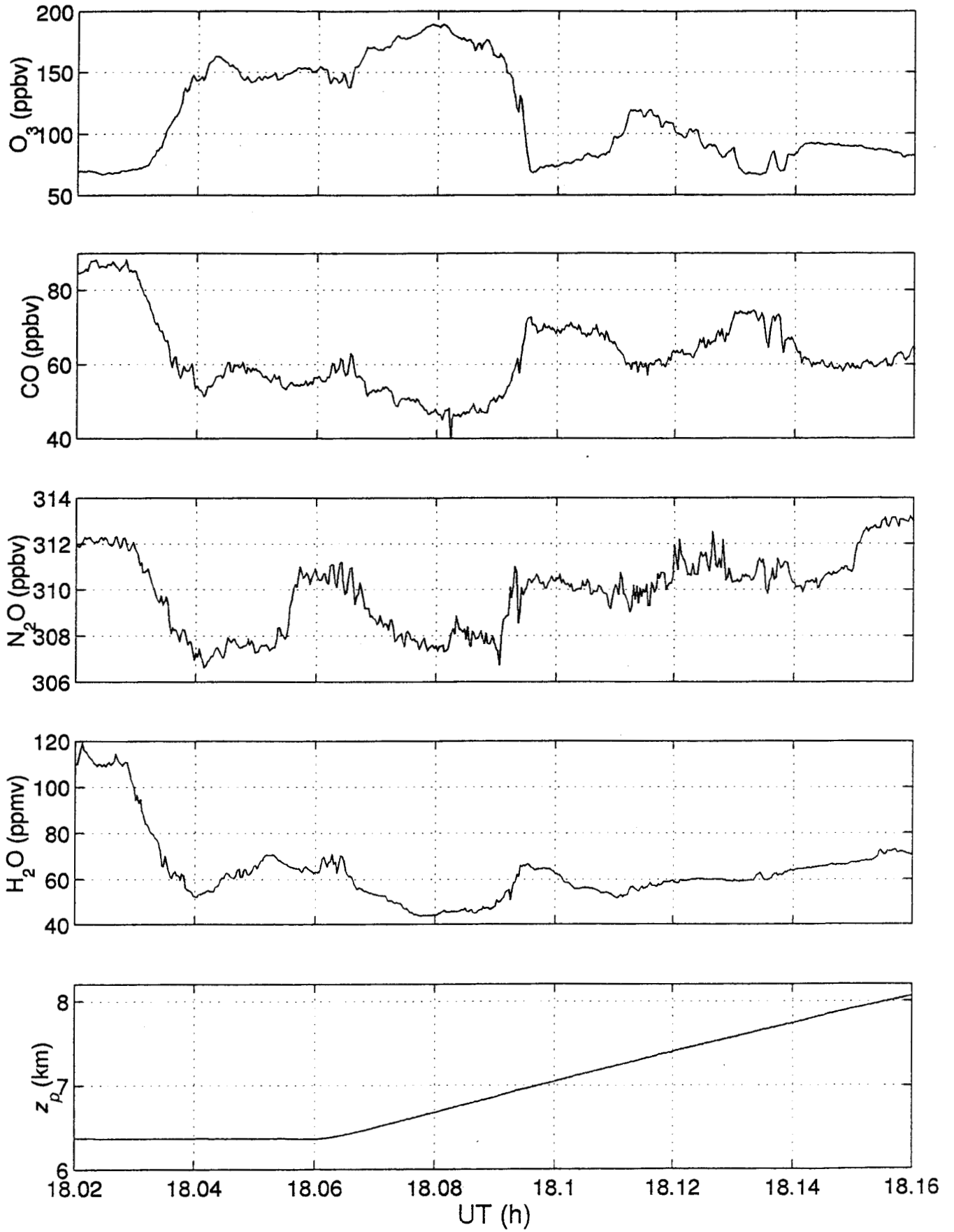


Fig. 1

SONEX DC-8 1997/10/13

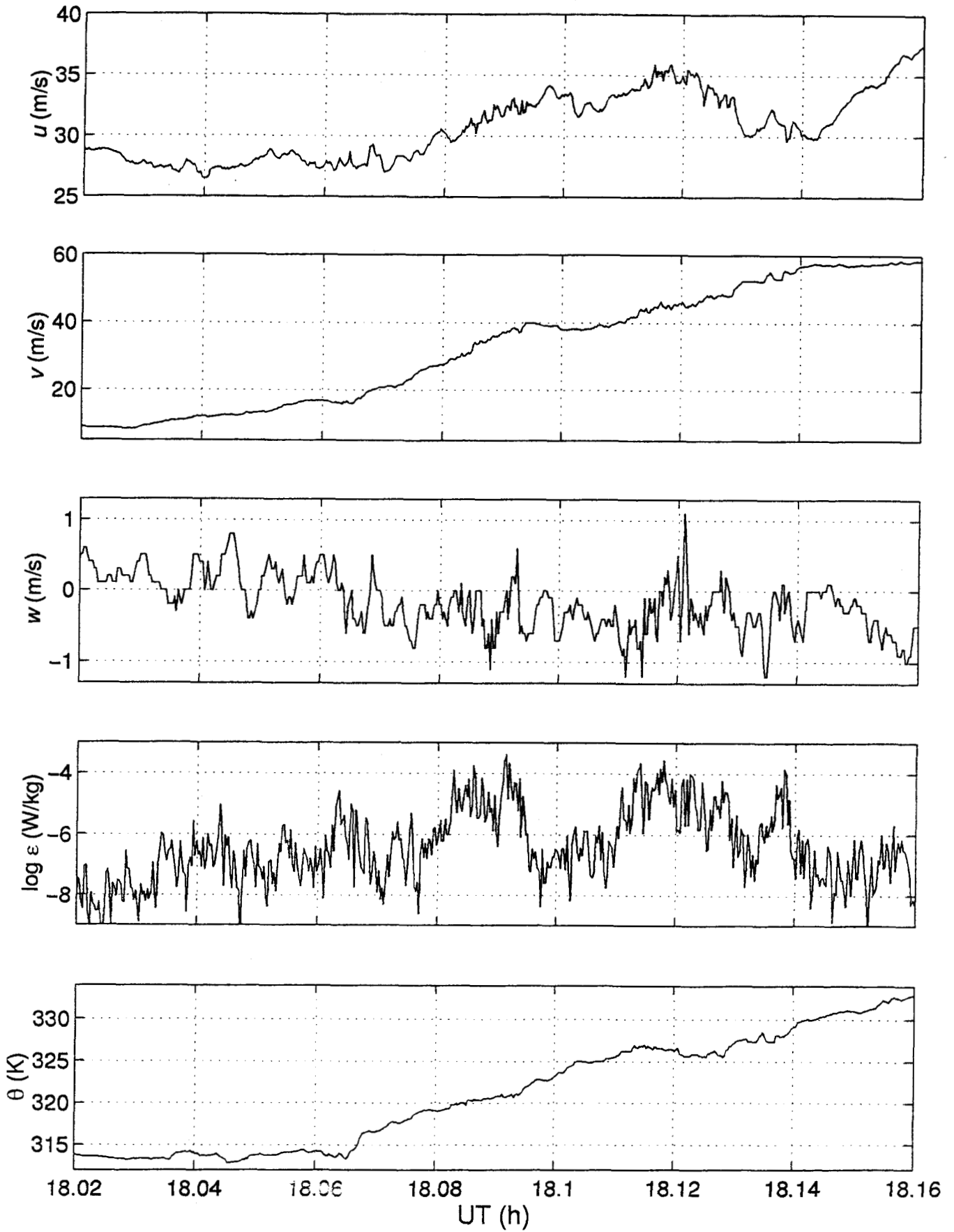


Fig. 2

SONEX DC-8 1997/10/13

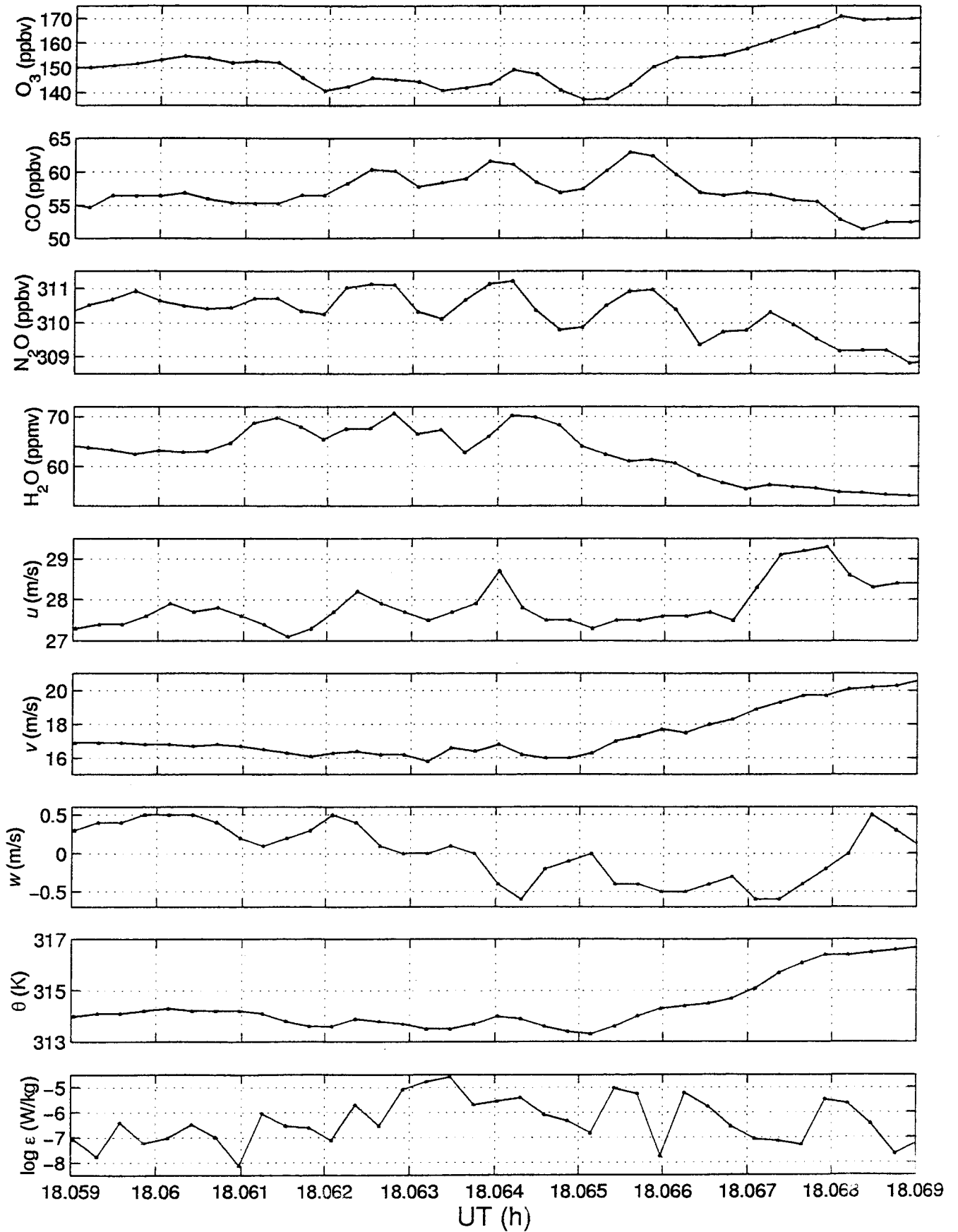


Fig. 3

SONEX DC-8 1997/10/13

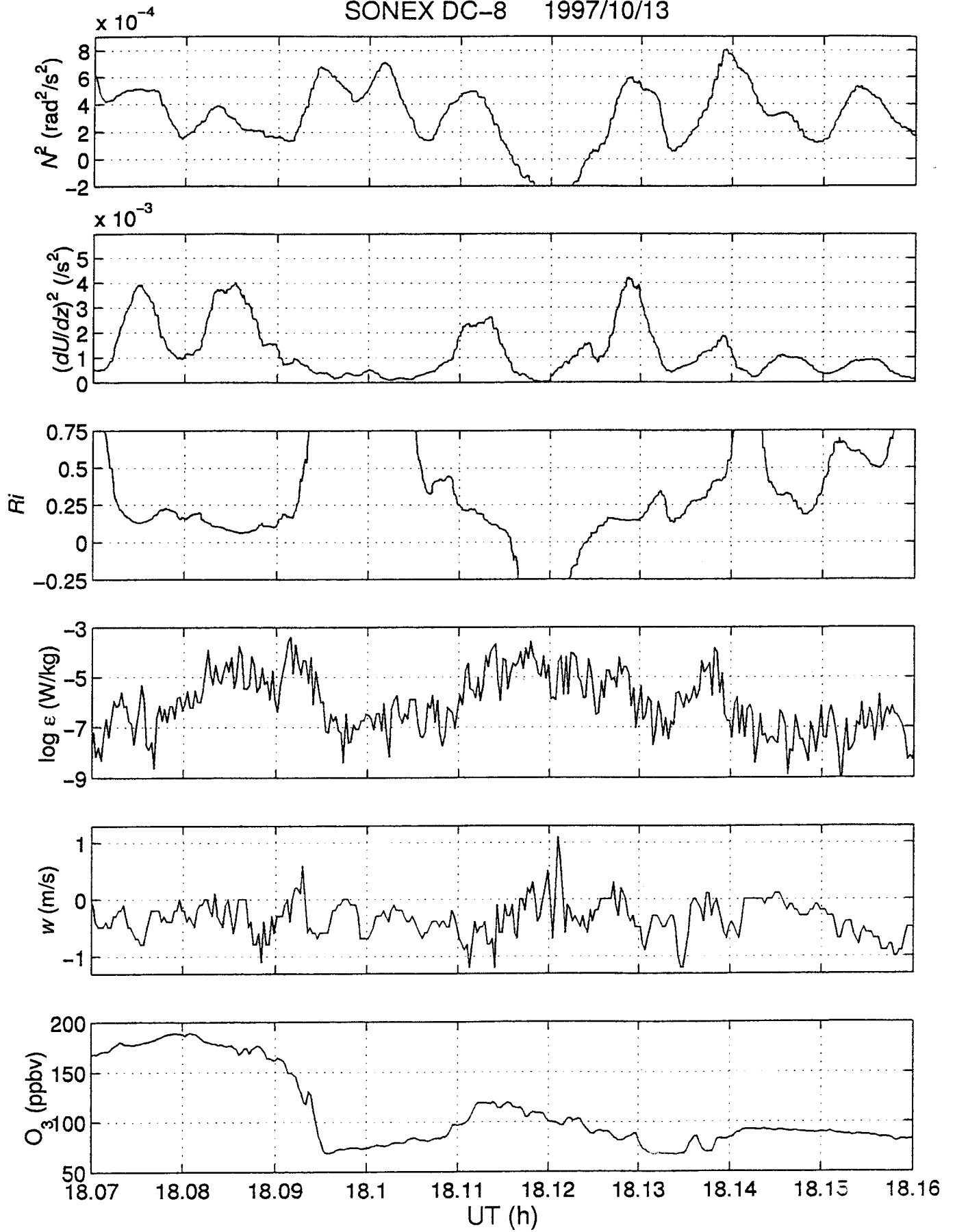


Fig. 4

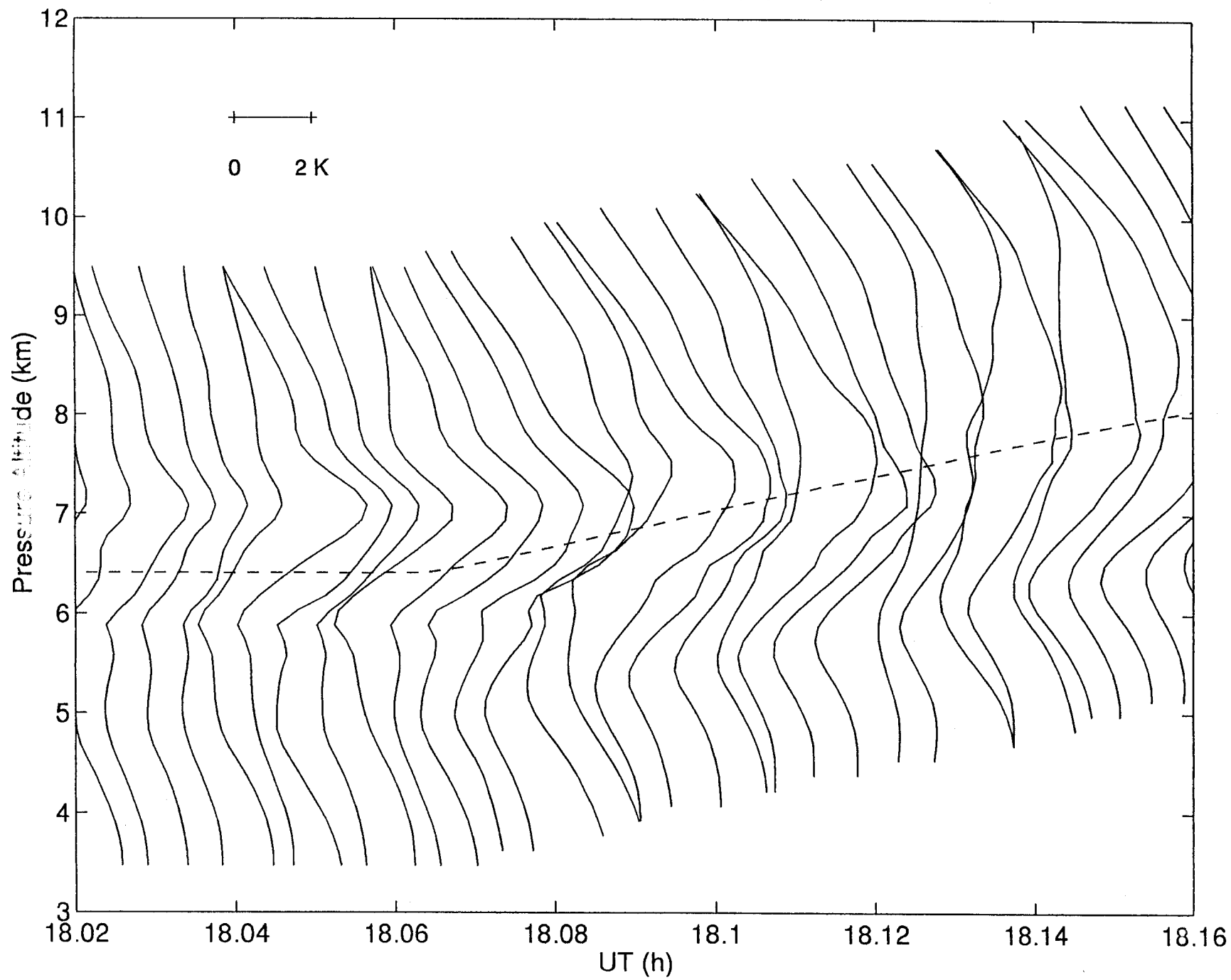


Fig. 5

SONEX DC-8 1997/10/13

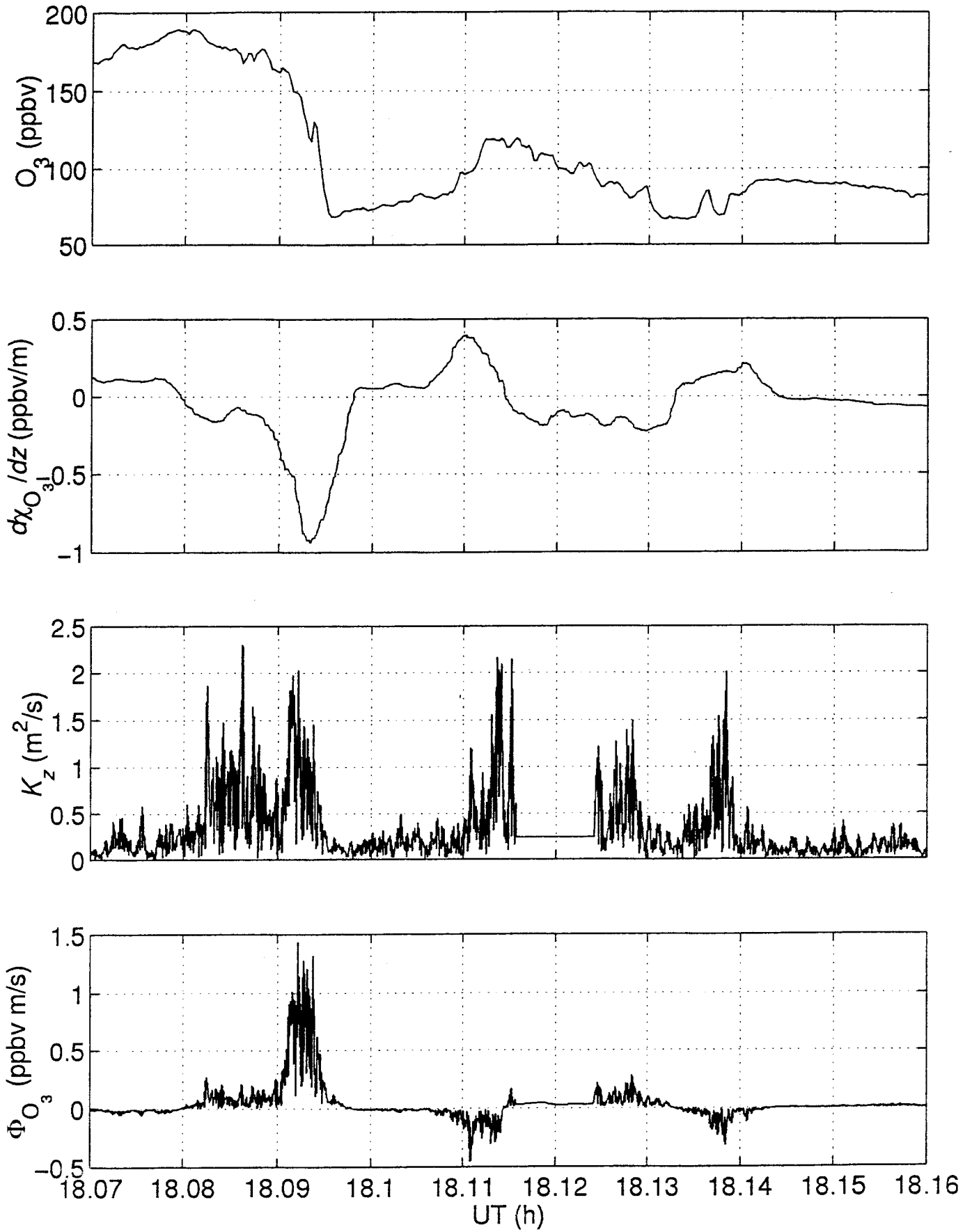


Fig. 6

SONEX DC-8 1997/10/15

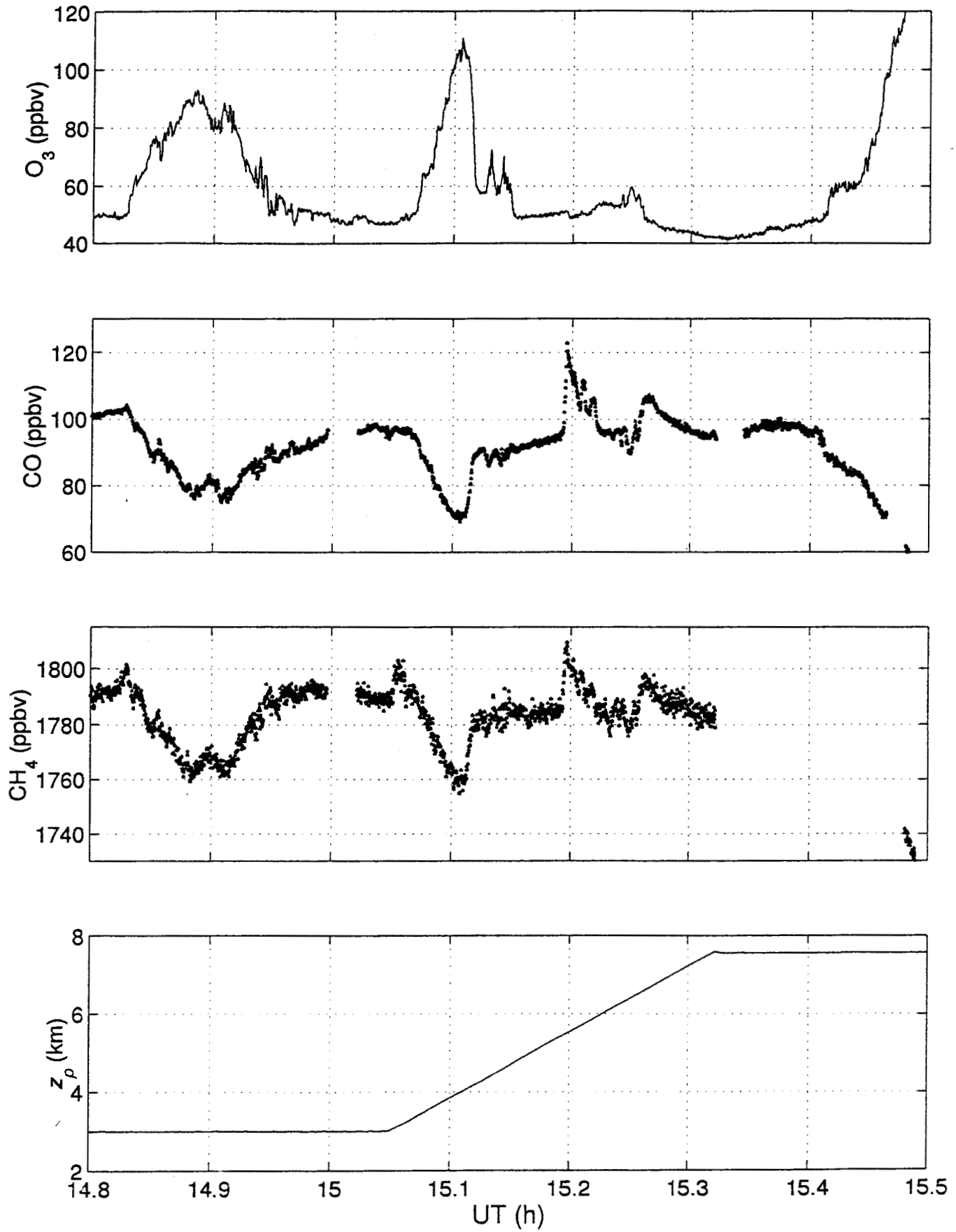


Fig. 7

SONEX DC-8 1997/10/15

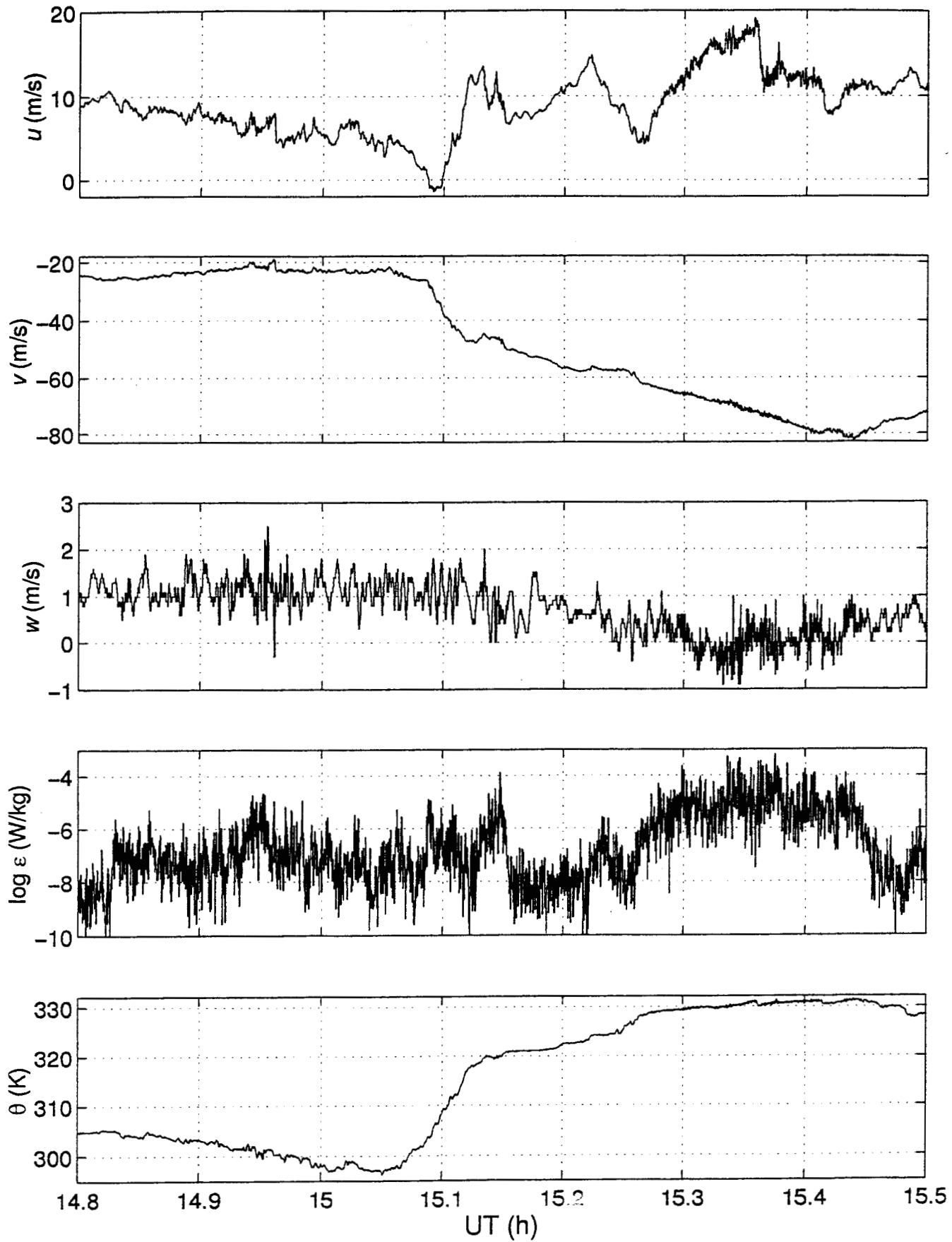


Fig. 8

SONEX DC-8 1997/10/15

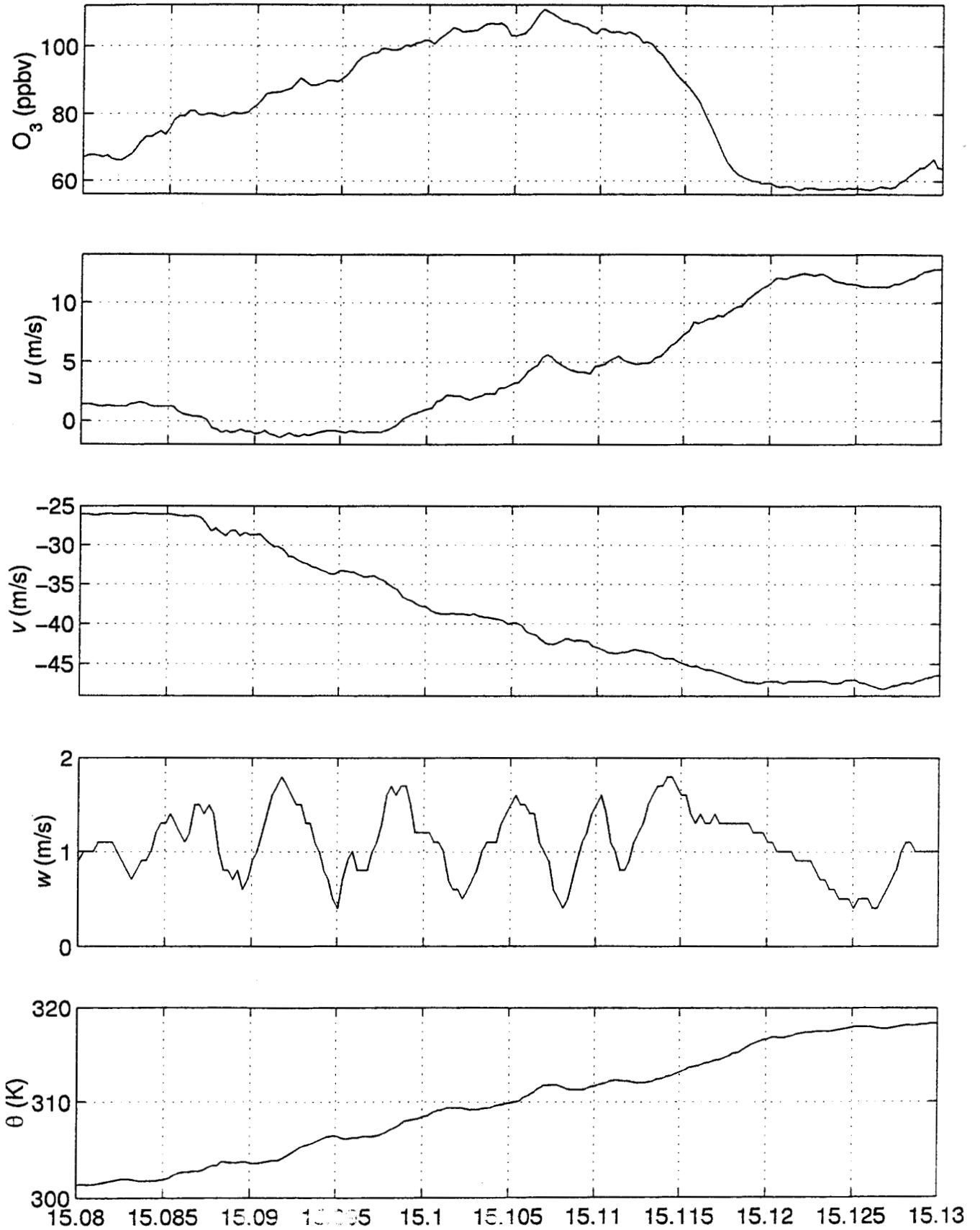


Fig. 9

SONEX DC-8 1997/10/15

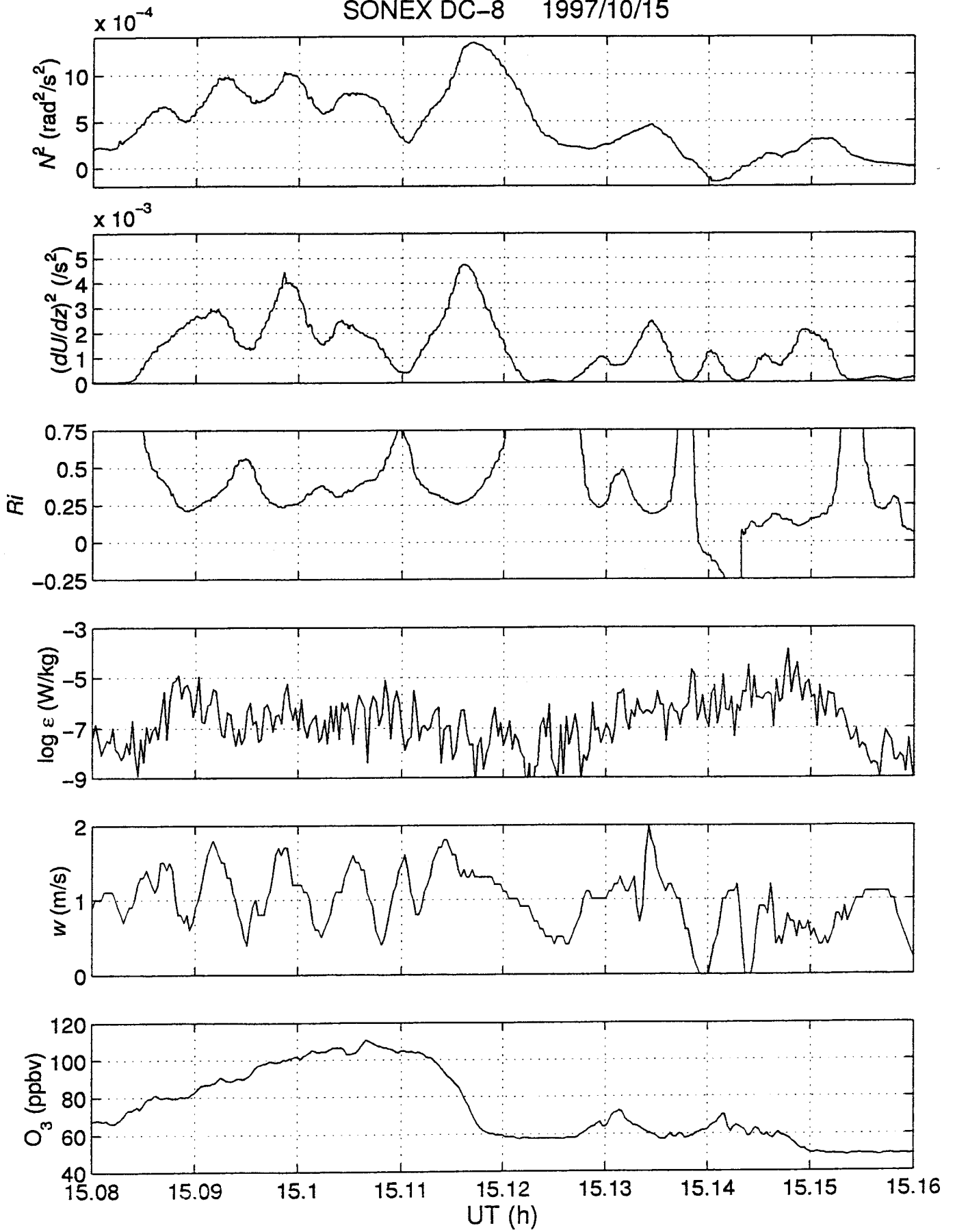


Fig. 10

SONEX DC-8 1997/10/15

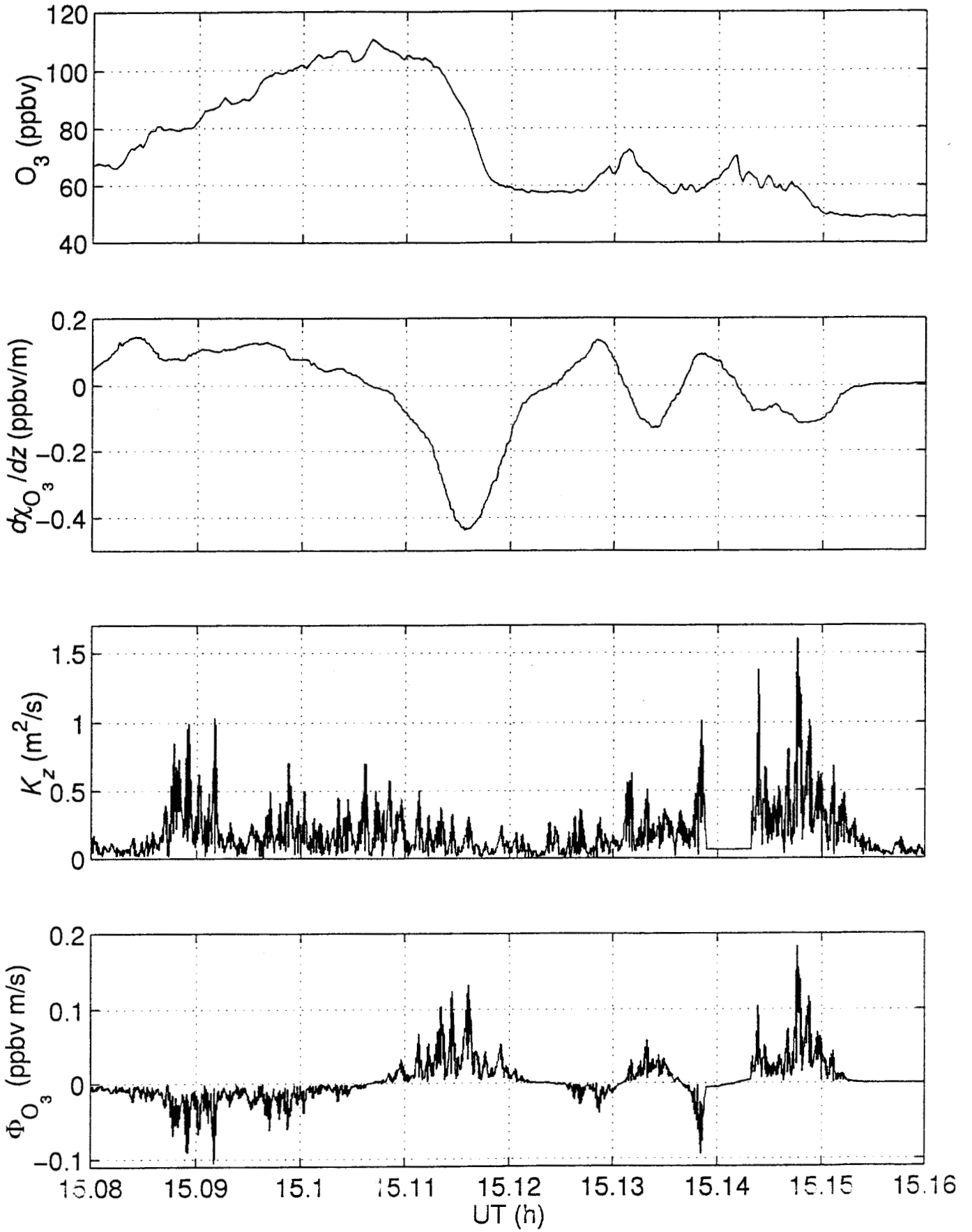
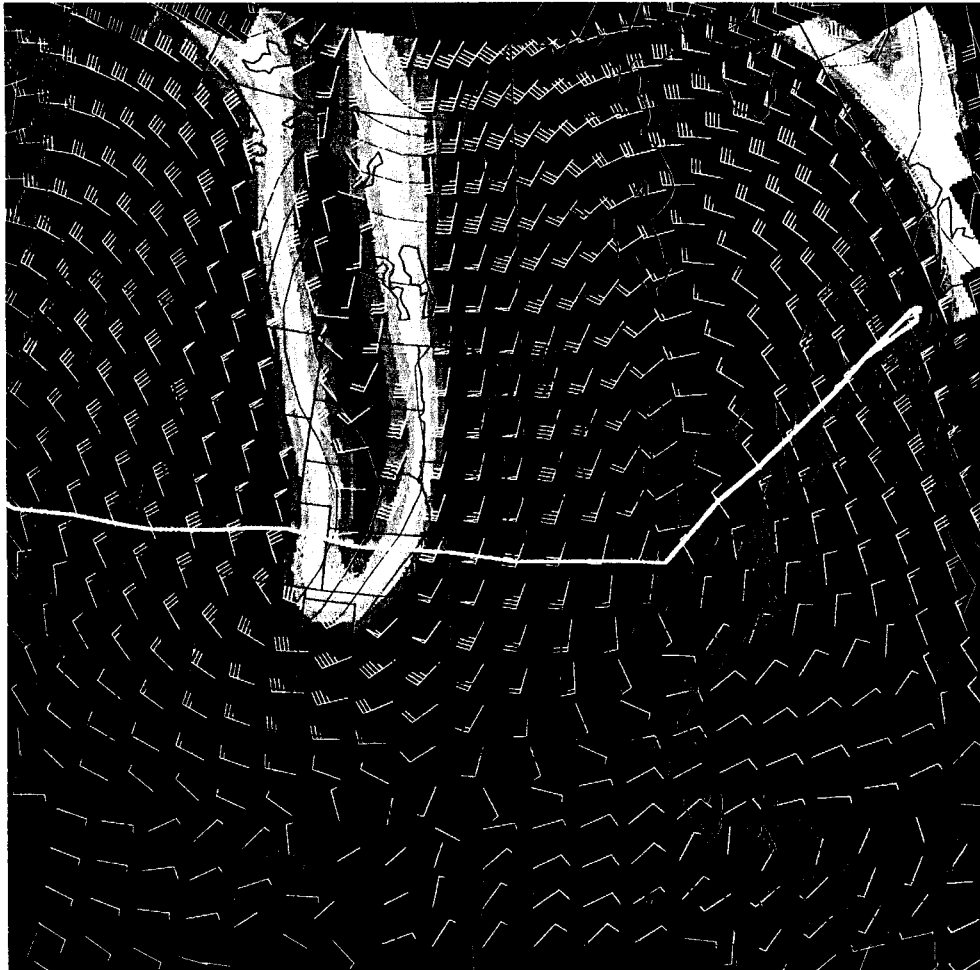


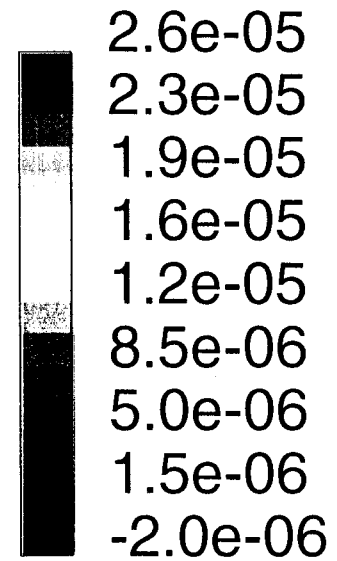
Fig. 11

12 UTC on 13 October, 1997 on the 330.0 K surface

ASM, Grid: GG2%5X2
Seq: STRATF, Spec: _



MPV ($\text{K m}^2/\text{kg s}$)



Z (gpm)

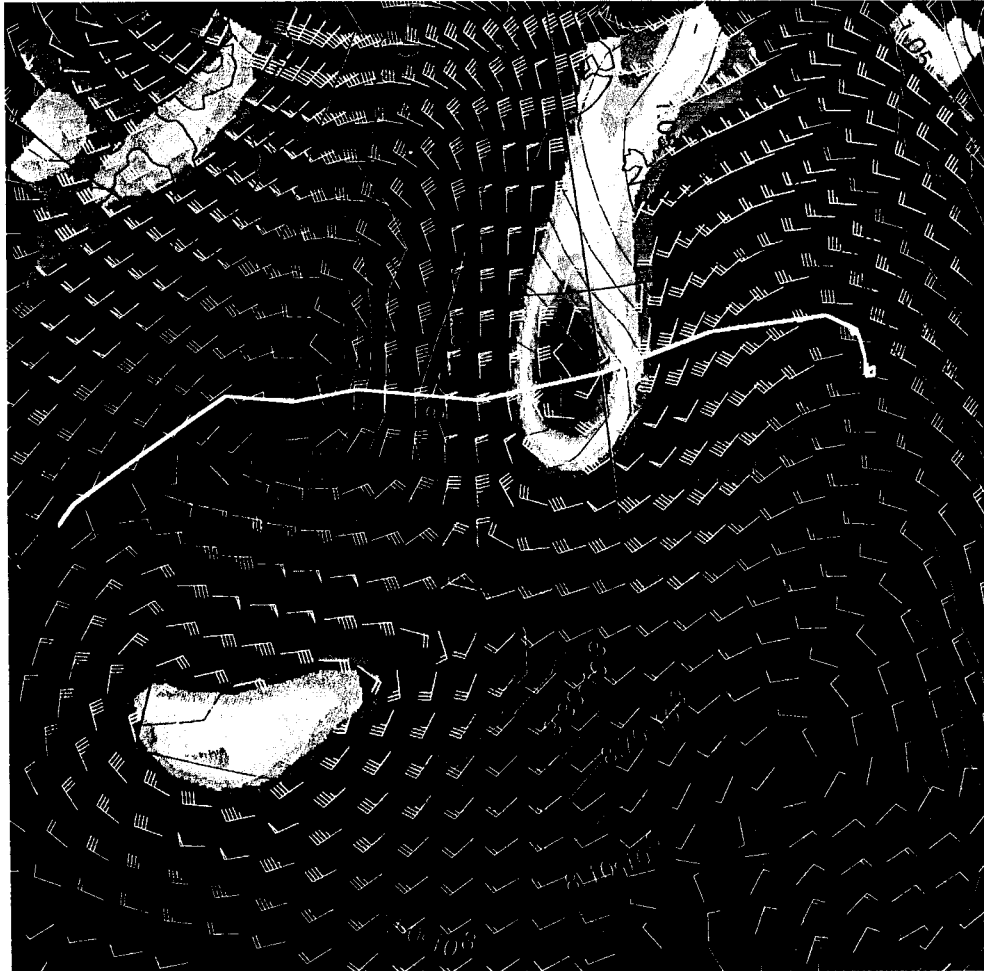
Plate 1

NASA

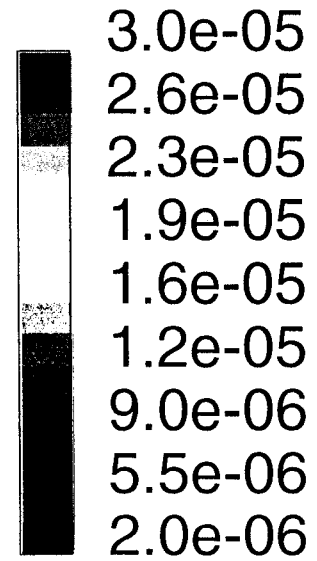
GSFC

12 UTC on 15 October, 1997 on the 330.0 K surface

ASM, Grid: GG2%5X2
Seq: STRATF, Spec: _



MPV ($\text{K m}^2/\text{kg s}$)



Z (gpm)

Plate 2

NASA
GSFC

SONEX DC-8 1997/10/13

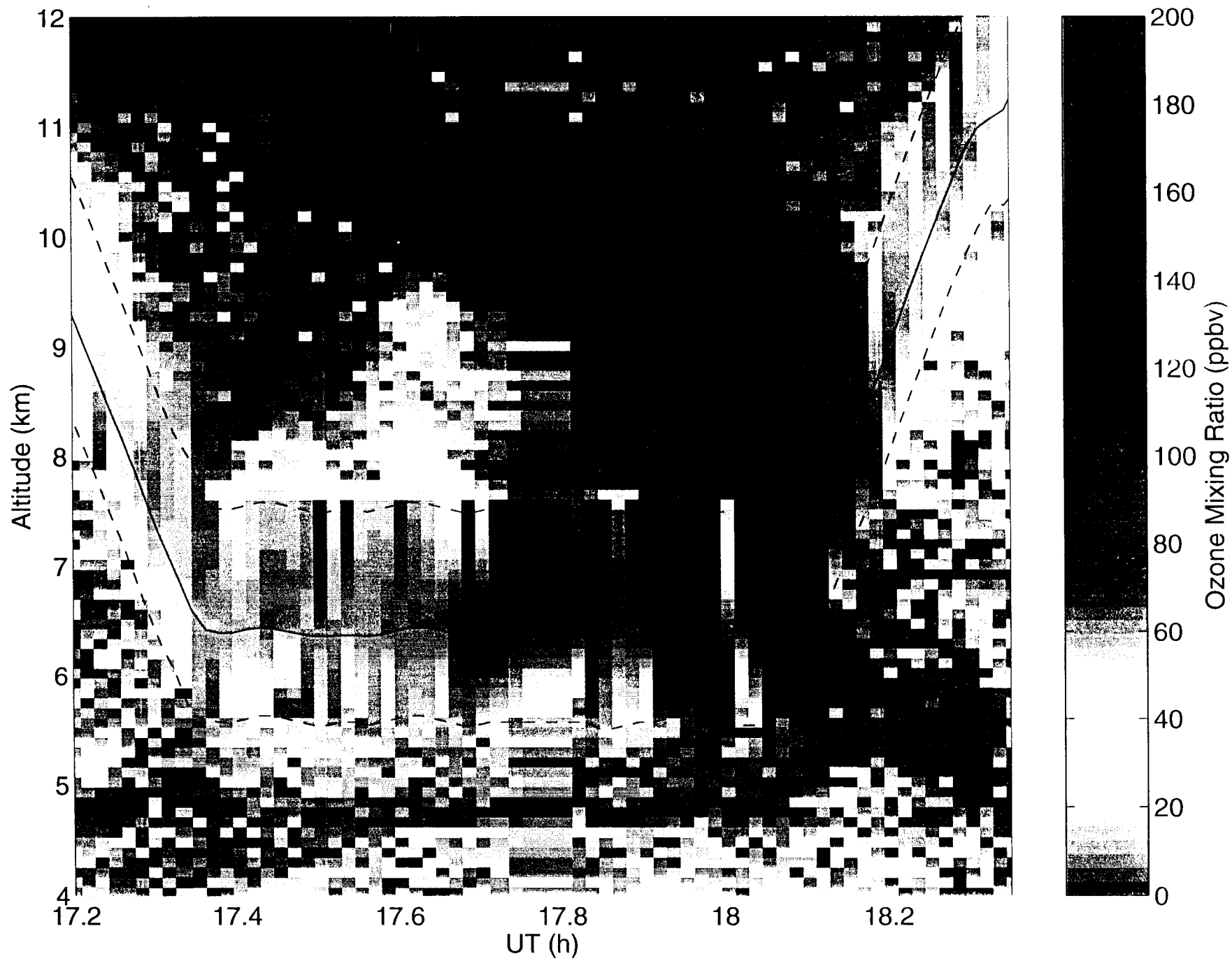


plate 3

SONEX DC-8 1997/10/15

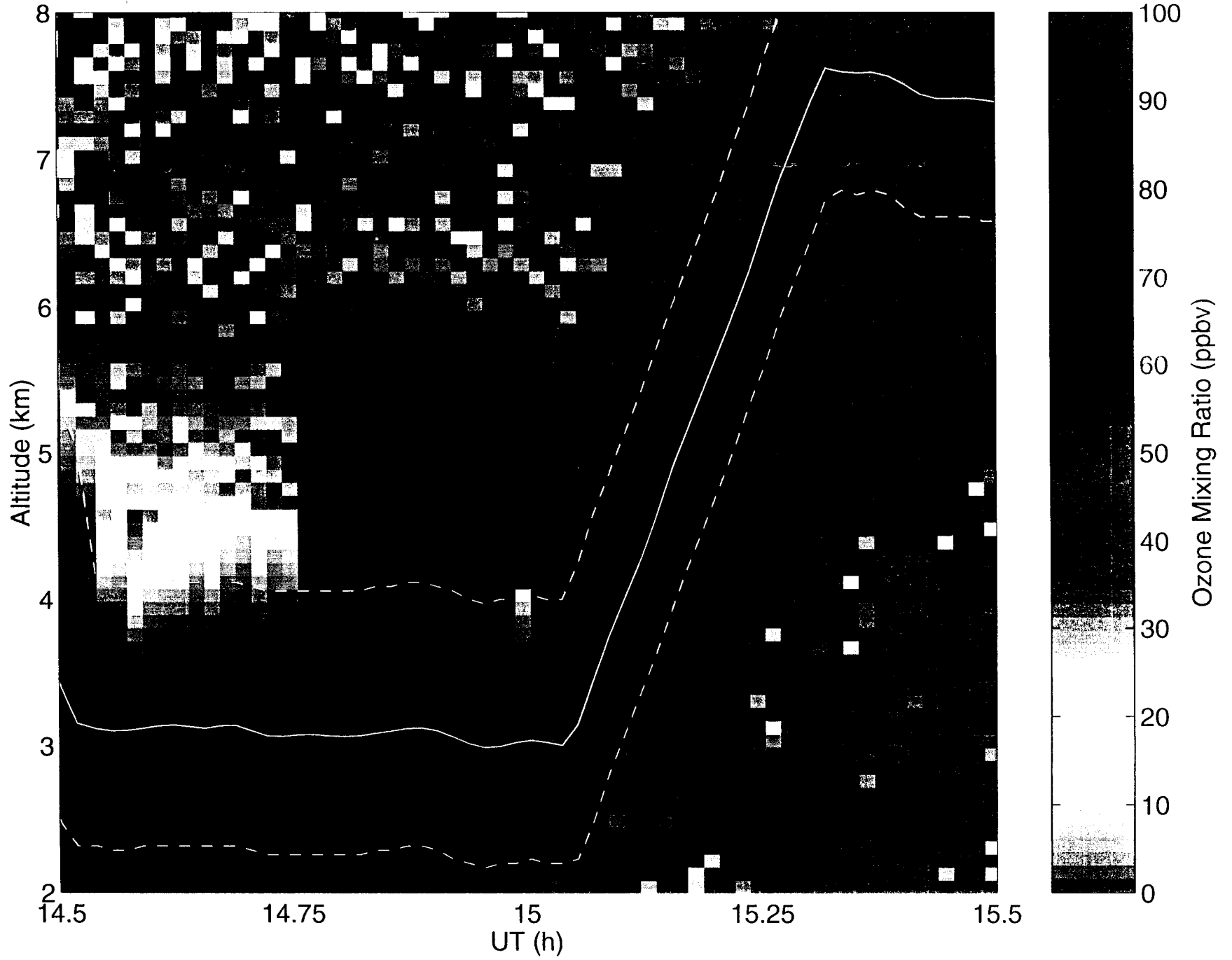


Plate 4

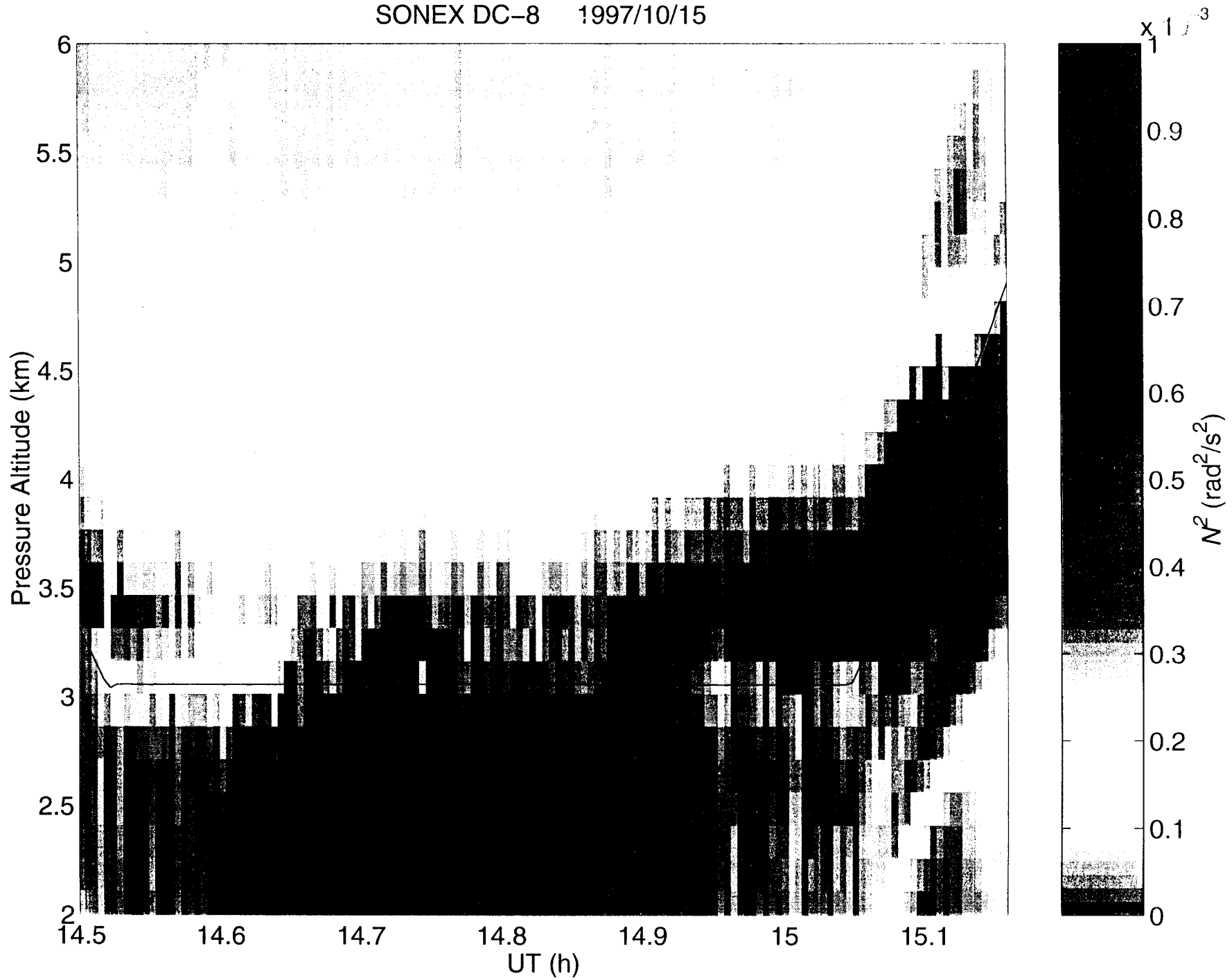


Plate 5